

A catalog of 1.58 million clusters of galaxies identified from the DESI Legacy Imaging Surveys

Z. L. WEN^{1,2} AND J. L. HAN^{1,2,3}

¹National Astronomical Observatories, Chinese Academy of Sciences, A20 Datun Road, Chaoyang District, Beijing 100101, China. hjl@nao.cas.cn

²CAS Key Laboratory of FAST, NAOC, Chinese Academy of Sciences

³School of Astronomy and Space Sciences, University of Chinese Academy of Sciences, Beijing 100049, China

ABSTRACT

Based on the DESI Legacy Imaging Surveys released data and available spectroscopic redshifts, we identify 1.58 million clusters of galaxies by searching for the overdensity of stellar mass distribution of galaxies within redshift slices around pre-selected massive galaxies, among which 877,806 clusters are found for the first time. The identified clusters have an equivalent mass of $M_{500} \geq 0.47 \times 10^{14} M_{\odot}$ with an uncertainty of 0.2 dex. The redshift distribution of clusters extends to $z \sim 1.5$, and 338,841 clusters have spectroscopic redshifts. Our cluster sample includes most of the rich optical clusters in previous catalogs, more than 95% massive Sunyaev-Zeldovich clusters and 90% ROSAT and eROSITA X-ray clusters. From the light distributions of member galaxies, we derive the dynamical state parameters for 28,038 rich clusters and find no significant evolution of the dynamical state with redshift. We find that the stellar mass of the brightest cluster galaxies grows by a factor of 2 since $z = 1$.

Keywords: galaxies: clusters: general — galaxies: distances and redshifts— galaxies: evolution

1. INTRODUCTION

As the largest virialized systems in the Universe, clusters of galaxies contain hundreds to thousands of galaxies, hot intracluster gas, and dark matter. They are tracers of large-scale structures and place powerful constraints on cosmological parameters (Allen et al. 2011; Böhringer et al. 2014; Hong et al. 2016). The dense environments and deep gravitational wells make galaxy clusters as an ideal laboratory for understanding galaxy formation (Liu et al. 2008; Wetzel et al. 2012), emission of intracluster medium (Rosati et al. 2002; Feretti et al. 2012) and the nature of dark matter (Markevitch et al. 2004; Banerjee et al. 2020).

Galaxy clusters can be identified as the over-density peaks of the galaxy distribution in optical/infrared images (Abell 1958), or detected by the X-ray emission of hot intracluster medium (Cavaliere & Fusco-Femiano 1976) or via the Sunyaev-Zeldovich (SZ, Sunyaev & Zeldovich 1972) signals in millimeter bands. The optical photometric surveys provide a large number of galaxy clusters. In the early years, about ten thousand nearby clusters were recognized from the single-band images of the Palomar Observatory Sky Survey (Zwicky et al. 1963; Abell et al. 1989; Gal et al. 2003; Lopes et al. 2004). When multi-band data of the Sloan Digital Sky Survey (SDSS) are available, more than 150,000 galaxy clusters have been identified at redshifts $z < 0.8$ based on the red sequence of cluster member galaxies (Koester et al. 2007; Hao et al. 2010; Rykoff et al.

2014; Oguri 2014) or photometric redshifts of galaxies (Wen et al. 2009, 2012; Szabo et al. 2011; Wen & Han 2015; Banerjee et al. 2018). More clusters of galaxies were found from the deeper data of Hyper Suprime-Cam Subaru Strategic Program, Dark Energy Survey and Wide-field Infrared Survey Explorer (WISE) in the redshift range up to $z \sim 1.5$ (Oguri et al. 2018; Wen & Han 2021, 2022; Aguena et al. 2021; Thongkham et al. 2024).

Recently, the Dark Energy Spectroscopic Instrument (DESI) Legacy Surveys¹ have been carried out and released data in three optical bands (g -band, r -band, and z -band²) with one magnitude deeper than the SDSS (Dey et al. 2019). Incorporating the public DECam data, the DESI Legacy Surveys cover a sky area of more than 20,000 deg². Several large cluster catalogs have been published based on previous DESI data release 9 (DR9) (Yang et al. 2021; Zou et al. 2022; Yantovski-Barth et al. 2023). The latest DR10 data cover a larger sky area with some overlapped areas in the DR9 and include new i -band data from the NOIRLab Data Archive, an excellent database for identifying a larger sample of clusters to higher redshifts.

Following our previous work (Wen et al. 2009, 2012; Wen & Han 2015, 2021, 2022), in this paper we identify 1.58

¹ <https://www.legacysurvey.org/>

² We use z for redshift in this paper and z_m for the z -band magnitude to avoid confusion.

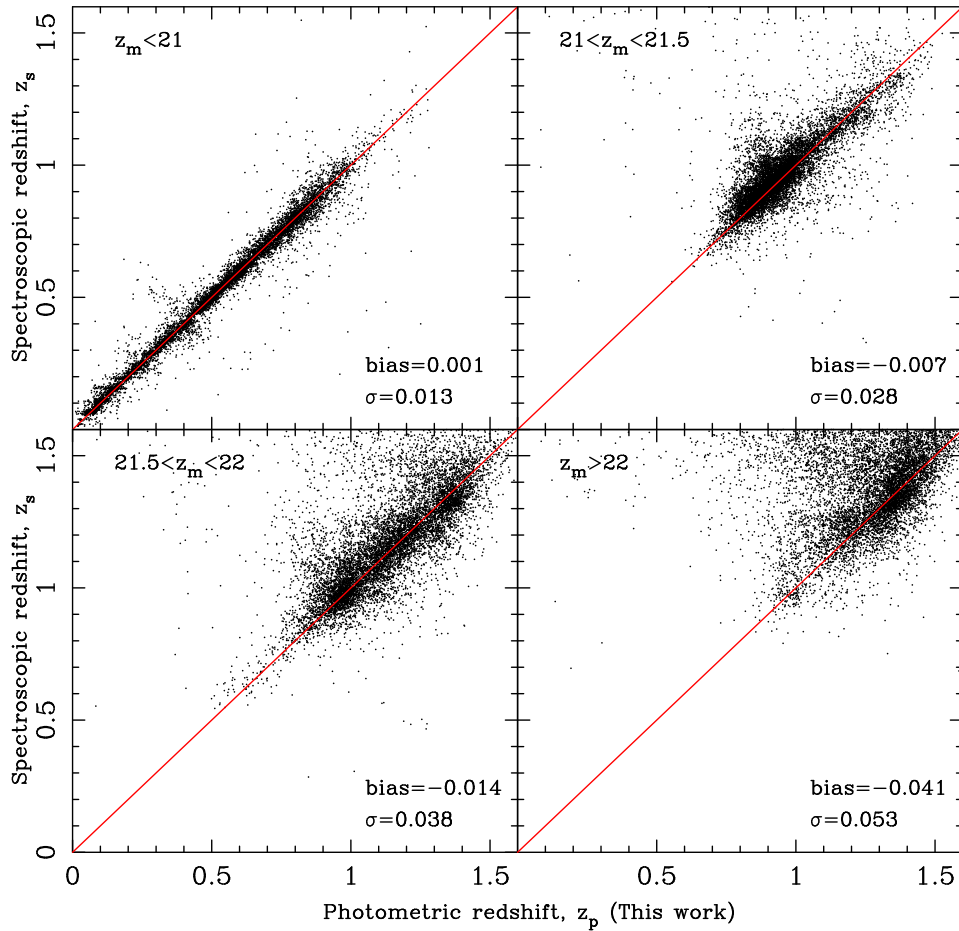


Figure 1. Comparison between the newly estimated photometric redshifts z_p and spectroscopic redshifts z_s for galaxies in the region of middle survey depth and in four z -band magnitude ranges with different uncertainty and systematic bias as marked in each panel, where only randomly selected 10,000 galaxies are taken for plotting.

million galaxy clusters from the DESI Legacy Surveys released data by using photometric and available spectroscopic redshifts of galaxies. We first estimate photometric redshifts for galaxies with $griz$ data from the DESI Legacy Surveys and mid-infrared data from the WISE (Wright et al. 2010), as shown in Section 2. Details for identifying galaxy clusters and evaluating their physical parameters are given in Section 3. The comparisons with previously known clusters in the optical, X-ray, and SZ cluster catalogs are presented in Section 4. Cluster properties such as dynamical states and the stellar mass of the brightest cluster galaxies (BCGs) are discussed in Section 5. A summary is given in Section 6.

Throughout this paper, we assume a flat Lambda cold dark matter cosmology taking $H_0 = 70 \text{ km s}^{-1} \text{ Mpc}^{-1}$, $\Omega_m = 0.3$, and $\Omega_\Lambda = 0.7$. All magnitudes are given in the AB system.

2. SURVEY DATA FOR GALAXIES

The DESI Legacy Imaging Surveys (Dey et al. 2019) consist of three projects including the Dark Energy Camera Legacy Survey (DECaLS), the Beijing-Arizona Sky Survey

(BASS), and the Mayall z -band Legacy Survey (MzLS). The BASS and MzLS observe the northern hemisphere of Dec. $\geq 32^\circ$ with the survey magnitude depths of $g = 24.0$, $r = 23.5$ and $z_m = 22.9$, respectively, for point sources. The DECaLS covers the south hemisphere of Dec. $< 32^\circ$ with the magnitude depths of $g = 24.5$, $r = 23.9$ and $z_m = 22.9$, respectively, deeper than the northern part (Zou et al. 2019). The southern survey part also includes the data from the Dark Energy Survey (DES Abbott et al. 2021) with magnitude depths of $g = 25.3$, $r = 25.0$ and $z_m = 23.9$, respectively, the data from DECam Local Volume Exploration survey (Drlica-Wagner et al. 2022) with the depth of $z_m = 22.8$ and the data from DECam eROSITA survey³ with the depth of $z_m = 23.2$. The survey data in the DES region are deepest, have a middle depth in the north Galactic cap region with $-9.5^\circ \lesssim \text{Dec.} < 32^\circ$, and are shallowest in the rest sky regions. The DESI Legacy Surveys data are supplemented with

³ <https://noirlab.edu/science/programs/ctio/instruments/Dark-Energy-Camera/DeROSITAS>

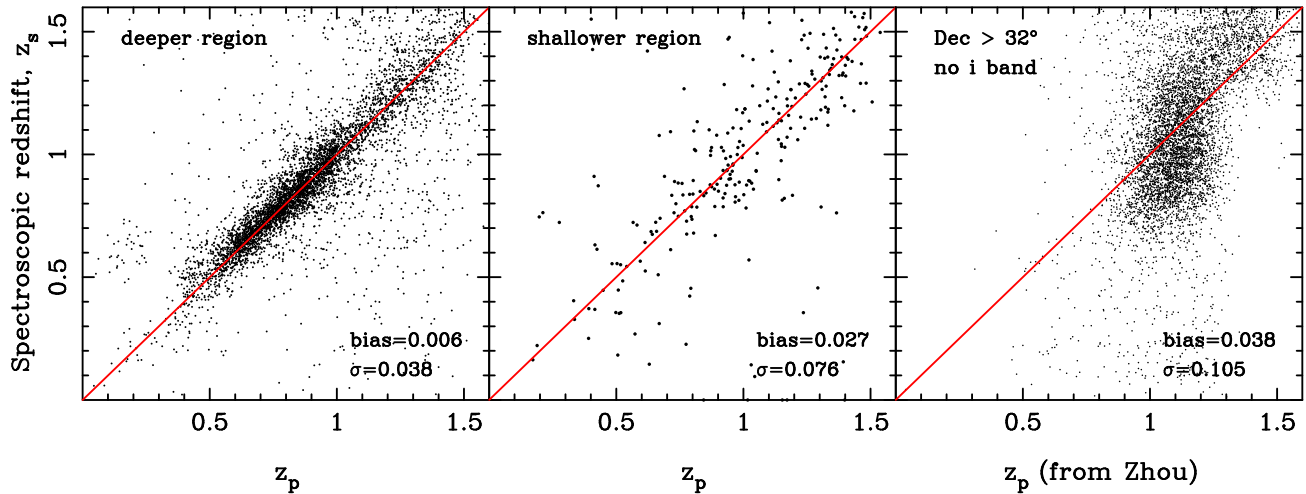


Figure 2. Comparison of photometric redshifts z_p with spectroscopic redshifts z_s for the faint galaxies of $z_m > 22$ in the deeper region (*the left panel*) and galaxies in the shallower region (*the middle panel*). *The right panel* is plotted for the galaxies in the shallower region of $\text{Dec} \geq 32^\circ$ without i -band data, and the values of z_p are directly taken from Zhou et al. (2021). The uncertainty and systematic bias are marked in each subpanel.

the mid-infrared co-added imaging data from the unWISE (Lang 2014; Schlafly et al. 2019) with magnitude depths of $W1 = 20.4$ and $W2 = 19.5$, respectively.

The DESI Legacy Surveys DR9 contains the photometric data in the grz and $W1W2$ bands covering a sky area of about $19,700 \text{ deg}^2$. The DR10 published data for objects from the DECaLS in the newly observed regions and also new i -band data for objects in some southern parts of DR9, covering a sky area of about $15,300 \text{ deg}^2$ with six bands ($grizW1W2$). Current DESI Legacy Surveys have released data in a total sky area of about $24,000 \text{ deg}^2$.

We analyze the DR9 and DR10 data independently for cluster identification in this work because of the different number of bands and choose the galaxy-type sources with $\text{TYPE} \neq \text{PSF}$. The sources with bad photometry are discarded by using the following quality flags (Yang et al. 2021): $\text{FRAFLUX} < 0.5$, $\text{FRACMASKED} < 0.4$ and $\text{FRACIN} > 0.3$ in both the grz for the DR9 data and the $griz$ for the DR10 data. We also set a detection signal-to-noise of $S/N \geq 5$ in the $grzW1$ for the DR9 galaxies and $grizW1$ for the DR10 galaxies. Some classified galaxies by their morphology are faint contaminated stars, which can be partly removed in the color-color space (Zhou et al. 2023) by setting $r - z_m \geq 1$ and $z_m - W1 > 1.2(r - z_m) - 1.5$. Even so, some faint stars of $r - z_m < 1$ can not be distinguished from low redshifts galaxies. Fortunately they will not affect our cluster identification work because we use only massive galaxies and there are only a small number of such faint contaminated objects.

2.1. Spectroscopic redshifts of galaxies

Redshift of galaxies is a fundamental parameter for cluster identification in our algorithm (Wen & Han 2021, 2022).

We adopt spectroscopic redshifts of galaxies if they are available in the Two Micron All-Sky Survey (2MASS) Redshift Survey (Huchra et al. 2012), the SDSS DR17 (Abdurro’uf et al. 2022) and the early data release of the DESI (DESI Collaboration et al. 2023). These three redshift surveys give spectroscopic redshifts for 3.1 million galaxies in the DESI Legacy Surveys, which provide accurate redshifts for a large number of member galaxies for cluster identification.

2.2. Photometric redshifts of galaxies

The DESI Legacy Surveys DR9 includes photometric redshifts of galaxies estimated by the random-forest algorithm using the $grzW1W2$ magnitude data (Zhou et al. 2021). We adopt these photometric redshifts for 361.1 million galaxies in the DESI Legacy Surveys DR9.

Following our previous papers (Wen & Han 2021, 2022), we estimate photometric redshifts for galaxies in DR10 by using the nearest-neighbor algorithm, which is based on the empirical relation between galaxy colors and spectroscopic redshifts from a training sample. In the color spaces, the close neighbors of galaxies have a similar redshift. We calculate the distances in the color spaces between a targeted galaxy and all galaxies in the training sample. The photometric redshift of a targeted galaxy, z_p , is estimated to be the median spectroscopic redshift of the 20 nearest neighbors. The uncertainty of the photometric redshift, σ_{z_p} , is taken as the dispersion of these 20 spectroscopic redshifts.

For this work, we get a training sample of 883,000 galaxies with spectroscopic redshifts from the compiled data in Wen & Han (2021) and Wen & Han (2022), and also galax-

Table 1. The magnitudes, the estimated photometric redshifts and stellar masses for galaxies in the DESI Legacy Surveys DR10. The whole catalog is available at http://zmtt.bao.ac.cn/galaxy_clusters/.

R.A.	Dec.	g	Err $_g$	r	Err $_r$	i	Err $_i$	z_m	Err $_z$	W1	Err $_{W1}$	W2	Err $_{W2}$	z_p	σ_{z_p}	z_s	$\log(M_*)$	Flag
(1)	(2)	(3)	(4)	(5)	(6)	(7)	(8)	(9)	(10)	(11)	(12)	(13)	(14)	(15)	(16)	(17)	(18)	(19)
0.00002	-3.25165	23.427	0.082	22.989	0.069	22.733	0.104	22.274	0.105	21.287	0.182	22.241	0.755	1.2361	0.0774	-1.0000	10.01	0
0.00002	-0.27648	22.125	0.022	20.862	0.008	20.376	0.010	19.980	0.011	18.289	0.050	18.404	0.050	0.4243	0.0976	-1.0000	10.74	0
0.00002	-4.90665	23.219	0.049	22.688	0.039	22.158	0.041	21.682	0.040	20.421	0.081	20.590	0.205	1.1038	0.0791	-1.0000	10.33	0
0.00004	-1.09510	25.457	0.324	23.719	0.082	22.701	0.074	21.971	0.052	20.371	0.081	20.360	0.172	0.9334	0.0540	-1.0000	10.44	0
0.00004	-0.29959	22.046	0.021	21.152	0.012	20.969	0.019	20.709	0.024	19.690	0.051	20.880	0.284	0.4200	0.0695	-1.0000	9.87	0
0.00004	-0.62148	27.064	1.062	24.269	0.152	23.076	0.098	22.659	0.107	20.965	0.133	21.070	0.310	0.7433	0.0578	-1.0000	10.02	0
0.00007	-1.58000	24.180	0.100	23.386	0.058	22.645	0.067	22.463	0.078	21.247	0.170	23.265	1.362	0.7738	0.0250	-1.0000	9.55	0
0.00007	-4.43194	24.089	0.127	23.726	0.112	23.331	0.129	22.532	0.102	20.560	0.094	20.393	0.180	1.4287	0.0960	-1.0000	10.65	0
0.00007	-4.18086	23.170	0.062	22.282	0.033	21.400	0.023	21.063	0.028	19.550	0.050	20.062	0.136	0.8275	0.0357	-1.0000	10.55	0
0.00008	-2.42179	24.655	0.142	23.533	0.065	22.633	0.067	22.079	0.057	20.779	0.119	20.912	0.285	0.8729	0.0767	-1.0000	10.15	0

NOTE— Descriptions of columns. Columns 1 and 2: Right Ascension (R.A. J2000) and Declination (Dec. J2000) of a galaxy (in degree); Columns 3–14: magnitudes and errors (AB system) in the *griz*W1W2 bands; Columns 15 and 16: photometric redshift and error; Column 17: spectroscopic redshift, -1.0000 means not available; Column 18: logarithm of stellar mass with M_* in unit of M_\odot ; Column 19: flag for BCG-like galaxy, “1” for yes, “0” for no.

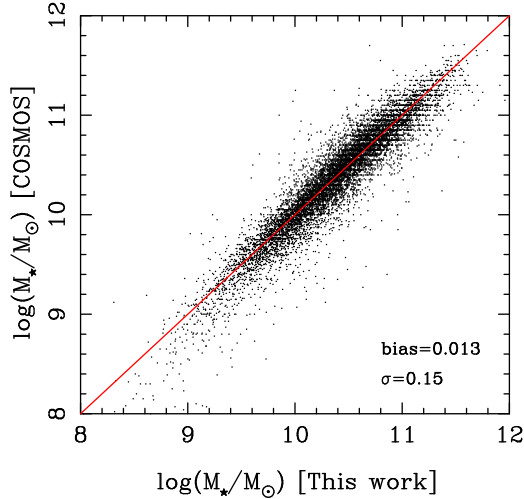


Figure 3. Comparison between our estimated stellar masses of galaxies with the values in the COSMOS2015 catalog.

ies from the flux-limited data in the Galaxy And Mass Assembly Survey (GAMA, Liske et al. 2015; Driver et al. 2022), VIPERS DR2 (Scodreggio et al. 2018) and DEEP2 (Matthews et al. 2013), plus the local galaxies in the 2MASS Redshift Survey (Huchra et al. 2012) and the galaxies in the early data release of the DESI (DESI Collaboration et al. 2023). The galaxies in this sample has a redshift in the range of $z < 1.6$.

We then estimate photometric redshifts for 295.6 million galaxies in the DESI Legacy Surveys DR10 with *griz*W1W2 magnitude data, see Table 1. In Figure 1, we compare the photometric redshifts with spectroscopic redshifts for galaxies with different z -band magnitudes in the region of middle survey depth. For bright galaxies of $z_m < 21$, the uncertainty of photometric redshifts, defined as $\sigma_{\Delta z} = 1.48 \times$

$\text{median}(|z_p - z_s|/(1 + z_s))$, is only about 0.013 for the galaxies at $z < 1$. The uncertainty increases to 0.028 for the galaxies of $21 < z_m < 21.5$ at $0.7 < z < 1.3$, and to 0.038 for the galaxies of $21.5 < z_m < 22$ at $0.9 < z < 1.5$. The photometric redshifts are reasonably estimated even for very faint galaxies of $z_m > 22$, with an uncertainty of only 0.053 and a fairly small systematic bias of -0.041 . The systematic bias and uncertainty are larger for fainter galaxies at $z > 1.2$, which are probably caused by the small number of faint galaxies at high redshifts in the training sample. Moreover, the 4000 Å break is moving out of the z_m band for objects of $z > 1.2$, making the estimate of photometric redshifts difficult. The survey depth does affect the accuracy of photometric redshifts, especially for faint galaxies. As seen in Figure 2, the photometric redshift is slightly more accurate in the deeper region and worse in the shallower region for galaxies of $z_m > 22$.

Based on the DESI Legacy Surveys DR9 data, Zhou et al. (2021) used the *grz*W1W2 magnitudes to estimate photometric redshifts. For galaxies of $z_m < 21$, the redshifts are well estimated with an uncertainty of about 0.01332, but not for fainter galaxies. For the galaxies of $z_m > 22$ in the shallow region of $\text{Dec.} \geq 32^\circ$, the photometric redshifts are systematically overestimated at $z_s < 1$ and underestimated at $z_s > 1$, with an uncertainty as large as 0.105 (see the right panel of Figure 2). We have tested our algorithm by ignoring the newly added *i*-band magnitude data for galaxies in the DR9 and DR10 and get the consistent results with Zhou et al. (2021). We therefore conclude that the newly added *i*-band data in the DR10 can significantly improve the accuracy of photometric redshift estimates.

In summary, we take photometric redshifts for 361.1 million galaxies from the DESI Legacy Surveys DR9, and also

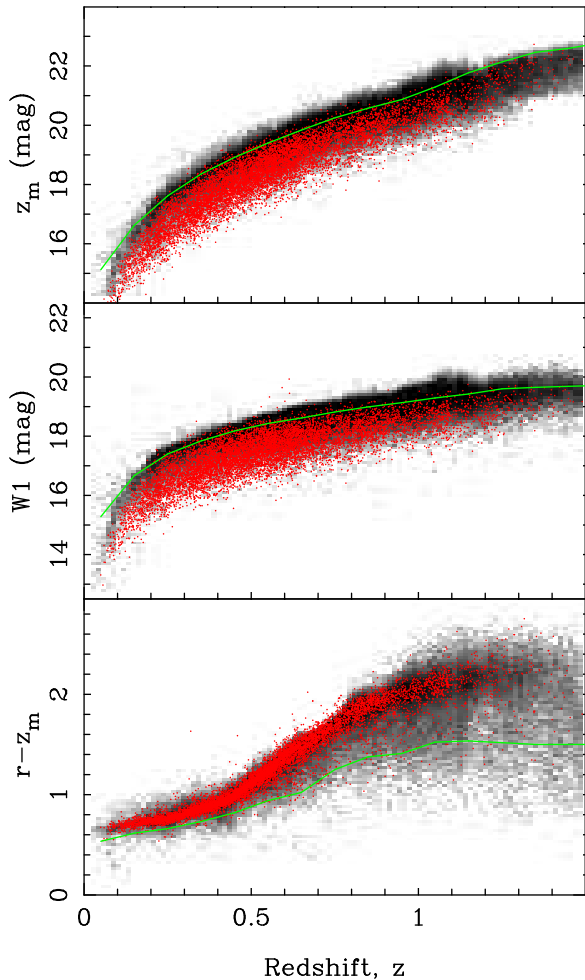


Figure 4. Magnitudes at z and W1 bands and color ($r - z_m$, bottom) against redshifts for 10,000 randomly-selected known BCGs, as indicated by small (red) dots. The distribution of all massive galaxies of $M_* \geq 10^{11} M_\odot$ in the DESI Legacy Surveys are shown with the number density in gray. We set criteria for BCG-like galaxies as shown by the solid line.

the newly estimated photometric redshifts for 295.6 million galaxies from the DR10 for cluster identification.

2.3. Stellar masses of galaxies

Stellar masses of galaxies are another fundamental parameter for cluster identification in our algorithm. The optical and infrared luminosities of galaxies are good tracers of their stellar mass (Bell et al. 2003; Kauffmann et al. 2003; Wen et al. 2013). In Wen & Han (2021), we took the values from the COSMOS2015 catalog (Laigle et al. 2016) to calibrate the relation between the W1-band luminosity, the color $r - z_m$, and the stellar mass of galaxies. Here, we do a similar calibration but for the relation of the stellar mass with the z -band luminosity. We then obtain two kinds of stellar mass estimates for galaxies from the W1 and z -band luminosities separately and then take the average. The final values are

listed in Column (18) of Table 1. Compared to the stellar masses of galaxies in the COSMOS2015 catalog, our newly estimated masses have an uncertainty of only 0.15 dex (Figure 3), much improved from the single W1 band (Wen & Han 2021).

3. GALAXY CLUSTERS IDENTIFIED FROM THE DESI LEGACY SURVEYS

In optical, galaxy clusters show a distinct overdensity of galaxies around a massive central galaxy. The total stellar mass of member galaxies is tightly related to cluster mass (Andreon 2010; Pillepich et al. 2018; Palmese et al. 2020). Using the photometric redshifts, we can select most of the member galaxies with a small fraction of contamination (Wen et al. 2009). Therefore, we identify galaxy clusters by searching for the overdensity of stellar mass within a photometric redshift slice around massive galaxies.

3.1. Pre-selection for BCG-like massive galaxies

Galaxies clusters generally contain one or more massive galaxies, and the central one is called the BCG. Pre-selection for BCG-like galaxies can help to identify galaxy clusters more efficiently.

As the most massive galaxies in the Universe, the BCGs are very luminous in the optical and infrared bands (Hansen et al. 2009). In general, they contain an old stellar population and show a red color (Whiley et al. 2008), and are located at the bright end in the magnitude–redshift diagram and at the red end in the color–redshift diagram (Wen et al. 2018). We select BCG-like massive galaxies based on the $rzW1$ magnitudes and the estimated redshift and stellar mass.

First, the BCG-like galaxies are selected to have a stellar mass of $M_* \geq 10^{11} M_\odot$ (Lidman et al. 2012; Wen & Han 2021). Then, according to the distributions of known BCGs from Abell clusters (Lauer et al. 2014), WHL and WH22 clusters (Wen et al. 2012; Wen & Han 2015, 2022), we set criteria shown in Figure 4, which cause a loss of 2.5% of the known faint BCGs but exclude many fainter galaxies detected in the z and W1 bands. Similarly, some blue massive galaxies are also discarded according to the threshold shown in the color–redshift diagram ($r - z_m$) in Figure 4. Note that BCGs at low redshifts has a tight distribution in colors, but these at high redshifts have much scattered colors due to star formation (O’Dea et al. 2008; Liu et al. 2012; McDonald et al. 2016; Wen & Han 2021).

In total, 15.23 million galaxies are pre-selected as possible BCGs, as indicated in Column (19) of Table 1, of which 9.40 million galaxies have i -band data.

3.2. Identification of galaxy clusters

Table 2. A catalog of 1.58 million clusters of galaxies identified from the DESI Legacy Surveys.

ID	Name	R.A.	Dec.	z_{c1}	flag $_z$	$z_{m,BCG}$	W1 $_{BCG}$	$\log(M_{*,BCG})$	r_{500}	λ_{500}	M_{500}	N_{gal}	Γ	σ_{Γ}	Source	Other catalog
(1)	(2)	(3)	(4)	(5)	(6)	(7)	(8)	(9)	(10)	(11)	(12)	(13)	(14)	(15)	(16)	(17)
1	J000000.1–372835	0.00046	–37.47628	0.1364	0	15.377	15.561	11.49	0.766	25.79	1.17	14	9.99	9.99	1	WHY18
2	WH-J000000.3–563518	0.00135	–56.58835	0.1957	0	15.712	15.723	11.70	0.625	23.24	1.06	7	9.99	9.99	1	
3	J000000.4–391925	0.00172	–39.32369	0.3580	0	17.713	17.313	11.41	0.526	15.90	0.73	7	9.99	9.99	1	Y21
4	J000000.5+021911	0.00201	2.31980	0.4282	1	18.043	17.359	11.55	0.612	23.40	1.07	13	9.99	9.99	1	redMaPPer
5	WH-J000000.6–590047	0.00260	–59.01297	0.1380	0	14.993	15.186	11.69	0.606	15.71	0.73	7	9.99	9.99	1	
6	J000000.8–412726	0.00327	–41.45719	0.4015	0	18.386	17.691	11.29	0.462	10.95	0.51	6	9.99	9.99	1	CFSFDP
7	J000001.0+012416	0.00403	1.40456	0.6538	1	18.611	17.088	11.85	0.560	24.77	1.13	6	9.99	9.99	1	CFSFDP
8	WH-J000001.0–594933	0.00426	–59.82570	0.6250	0	19.248	18.155	11.29	0.457	15.18	0.70	8	9.99	9.99	1	
9	J000001.0–535824	0.00435	–53.97320	0.6112	0	18.693	17.541	11.66	0.607	23.42	1.07	11	9.99	9.99	1	redMaPPer
10	J000001.2–030053	0.00504	–3.01485	0.5090	1	18.241	17.339	11.67	0.543	21.71	0.99	8	9.99	9.99	1	Y21

NOTE— Column 1: Cluster ID; Column 2: Cluster name with J2000 coordinates. Names with ‘WH’ are newly identified in this paper; Columns 3 and 4: Right Ascension (R.A. J2000) and Declination (Dec. J2000) of cluster BCG (in degree); Column 5: cluster redshift z_{c1} ; Column 6: redshift flag, ‘0’ for photometric redshift in Column 5 and ‘1’ for spectroscopic redshift; Columns 7–8: BCG magnitudes (AB system) in the z and W1 bands, respectively; Column 9: logarithm of BCG stellar mass with $M_{*,BCG}$ in unit of M_{\odot} ; Column 10: cluster radius, r_{500} , in Mpc; Column 11: cluster richness; Column 12: derived cluster mass, in units of $10^{14} M_{\odot}$; Column 13: number of member galaxy candidates within r_{500} ; Columns 14–15: relaxation parameter and error for rich clusters with $N_{gal} \geq 30$, otherwise 9.99 is given; Column 16: data source for the cluster. ‘1’ for the data with i -band magnitude available and ‘2’ for the data without i -band magnitude; Column 17: Reference notes for previously known clusters: maxBCG (Koester et al. 2007), WHL (Wen et al. 2009, 2012; Wen & Han 2015), GMBCG (Hao et al. 2010), AMF (Szabo et al. 2011; Banerjee et al. 2018), redMaPPer (Rykoff et al. 2014, 2016), CAMIRA (Oguri 2014), WHY18 (Wen et al. 2018), WH21 (Wen & Han 2021), Y21 (Yang et al. 2021), WaZP (Aguena et al. 2021), WH22 (Wen & Han 2022), CFSFDP (Zou et al. 2021, 2022), CluMPR (Yantovski-Barth et al. 2023).

(This table is available in its entirety in a machine-readable form.)

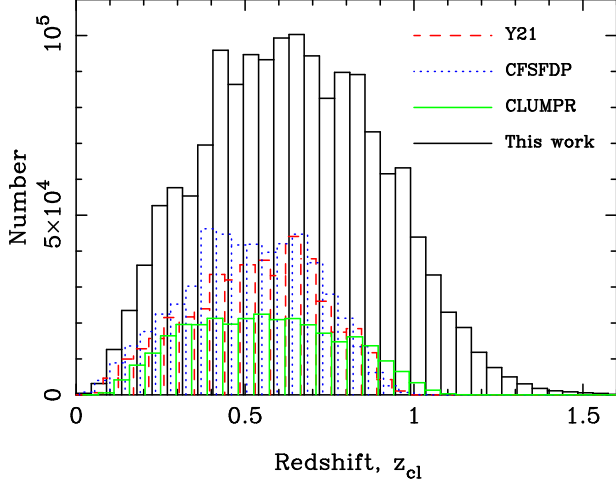


Figure 5. Redshift distribution of the identified 1,581,179 clusters, compared to clusters previously identified from DESI Legacy Surveys DR9 including Y21 (Yang et al. 2021), CFSFDP (Zou et al. 2022) and CLUMPR (Yantovski-Barth et al. 2023).

Following our previous works (Wen & Han 2021, 2022), we identify galaxy clusters by searching for the overdensity of stellar mass around massive galaxies within a redshift slice and then estimating the parameters of cluster candidates.

Previously, to get cluster radius and mass for to-be-identified galaxy clusters, we first calibrated the scaling relation between the total stellar mass within a given radius and cluster radius (r_{500}) or mass (M_{500}) by using a sample of M_{500} known clusters. Here, r_{500} is the radius within which the mean density is 500 times the critical density of the universe. M_{500} is the cluster mass within r_{500} . We took galaxies within a photometric redshift slice, $z \pm \Delta z$, around massive galaxies as member galaxy candidates for cluster candidates. The half of the slice thickness is taken as being

$$\Delta z = \begin{cases} 0.04(1+z) & \text{for } z \leq 0.7 \\ 0.15z - 0.037 & \text{for } z > 0.7 \end{cases}. \quad (1)$$

We discard the member galaxy candidates with a large redshift uncertainty of $\sigma_{zp} > 2\Delta z$. Then, we searched for galaxy cluster candidates from the whole photometric data. The redshift of the cluster candidate was estimated as the median value of photometric redshifts of member galaxy candidates. The cluster radius and richness (a mass proxy) were estimated according to the total stellar mass of member galaxy candidates and the calibrated scaling relations. A galaxy cluster is identified if it is above a richness threshold.

In this work, we make some improvements to our procedures. First, only massive galaxies with $M_* \geq 10^{10} M_\odot$ are used since they have a smaller redshift uncertainty than these less massive (and fainter) galaxies. The central BCGs of to-be-identified clusters are therefore only taken from the pre-selected BCG-like galaxies. Second, the spectroscopic

redshifts of some galaxies, if available, are used to determine the redshifts of cluster candidates and to label member galaxies. We adopt the available spectroscopic redshift of the BCG as the spectroscopic redshift of a cluster. If the spectroscopic redshift of the BCG is not available, the available spectroscopic redshifts of other galaxies are adopted if they are within $0.025(1+z)$ from the cluster photometric redshifts. The member galaxies with spectroscopic redshifts are determined if they have a velocity difference $\Delta v < 2500 \text{ km s}^{-1}$ from the cluster spectroscopic redshifts. Thirdly, we verify the scaling relations of r_{500} and M_{500} by using a large cluster sample (Wen & Han 2015), in which the cluster masses have been re-scaled for consistency and calibrated to weak lensing measurements (Vikhlinin et al. 2009). As done in our previous (Wen & Han 2021), we get the scaling relation for r_{500} as being

$$\log r_{500} = 0.402 \log \frac{M_{*,r1}}{10^{10} M_\odot} - (0.944 \pm 0.03) \\ + (0.43 \pm 0.02) \log(1+z), \quad (2)$$

where $M_{*,r1}$ is the total stellar mass (after background subtracted) of member galaxy candidates within a projected radius of $r_1 = 1.0 E(z)^{-1/3} \text{ Mpc}$. The total stellar mass, $M_{*,500}$, is then calculated from galaxies within a projected radius of r_{500} . We get the scaling relation between $M_{*,500}$ and cluster mass M_{500} , which is consistent with our previous result (Wen & Han 2021). The richness of a galaxy cluster, λ_{500} , is then defined as a redshift-independent mass proxy by

$$\lambda_{500} = M_{*,500}(1+z)^{0.21}/M_*^*, \quad (3)$$

where M_*^* is a characteristic stellar mass. A galaxy cluster is identified when it has a richness of $\lambda_{500} \geq 10$ and the number of member galaxy candidates within r_{500} as being $N_{\text{gal}} \geq 6$. The threshold is slightly lower than that we adopted in Wen & Han (2021) so that we do find more low-mass clusters.

After cleaning the repeated entries of identified clusters, we finally get 1,581,179 galaxy clusters, as listed in Table 2. Among them, 877,806 clusters are identified for the first time; 946,486 clusters are identified by using our newly obtained photometric redshifts, and the other 634,693 clusters are identified from photometric redshifts in the DESI Legacy Surveys DR9 data.

The redshift distribution of clusters extends to $z \sim 1.5$, and is compared to those clusters previously found from the DESI Legacy surveys DR9 (Yang et al. 2021; Zou et al. 2022; Yantovski-Barth et al. 2023), see Figure 5.

The sky distribution of galaxy clusters is shown in Figure 6. The clusters in the DES region in the south Galactic cap has the highest number density as being ~ 108 clusters per deg^2 . The density declines to ~ 80 clusters per deg^2 in

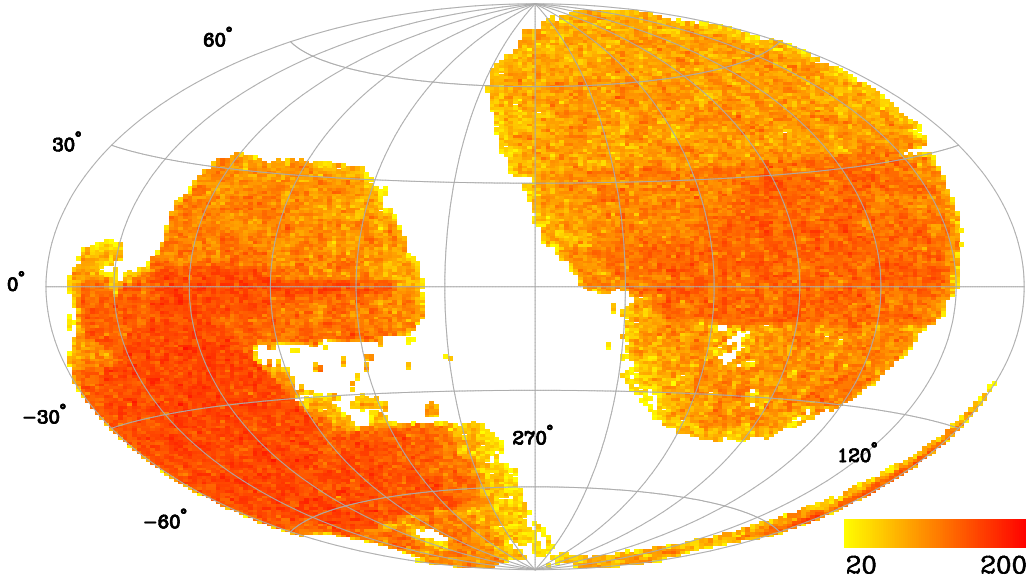


Figure 6. The sky distribution of identified galaxy clusters in the Equatorial coordinate system, expressed by the number of clusters per square degree.

the north Galactic cap region with $-9.5^\circ \lesssim \text{Dec.} < 32^\circ$, and to about ~ 50 clusters per deg^2 in the rest regions.

3.3. Verification of clusters and their parameters

To validate the reliability of identified clusters, we cross-match our identified clusters in the deep COSMOS field with previously known clusters. The COSMOS has a field of view of 2 deg^2 and more than 30-band deep imaging observations at the wavelengths from NUV (e.g. Zamojski et al. 2007), optical (e.g. Scoville et al. 2007; Taniguchi et al. 2007) to infrared (e.g. Sanders et al. 2007). Deep X-ray observations were also carried out for this sky area by the Chandra and XMM-Newton (e.g. Hasinger et al. 2007; Civano et al. 2016). Based on these high-quality data, galaxy clusters/groups have been identified with high completeness at low redshifts (Knobel et al. 2012; Wen & Han 2011; Söchtig et al. 2012; Wen & Han 2015; Darvish et al. 2017; Gozaliasl et al. 2019). Most of the clusters in the field have spectroscopic observations.

In the COSMOS field, we detect 221 clusters, 192 of which have counterparts in the previous catalogs. At $z < 0.9$, only four of 145 clusters are new. We carefully inspect all 221 clusters in the DESI color images and find that they all have a concentration of galaxies around their BCGs with a similar color. We conclude that our cluster sample has a high purity.

In our cluster sample, 338,841 clusters have spectroscopic redshifts for one or more galaxies. To test the accuracy of cluster photometric redshifts, we perform our algorithm by using photometric redshifts only for these clusters. Figure 7 shows the comparison between cluster photometric redshifts and spectroscopic redshifts. One can get the uncertainty of photometric redshift, $\sigma_z^{\text{cl}} = 1.48 \times \text{median}(|z_{\text{cl}} - z_s| / (1 +$

$z_s)) = 0.010$ for clusters identified from the data with available i -band magnitudes (see the left panel of Figure 7), which is $\sigma_z^{\text{cl}} = 0.012$ for the clusters identified from the data without i band in the shallowest region of $\text{Dec.} \geq 32^\circ$ (see the right panel of Figure 7).

Most member galaxy candidates are obtained by photometric redshifts, except for those with spectroscopic redshifts. The accuracy and completeness of the detected member galaxies are tested by using the spectroscopic survey data of $\sim 300,000$ galaxies from the GAMA survey down to flux-limited of $r < 19.8 \text{ mag}$ covering $\sim 286 \text{ deg}^2$ (Driver et al. 2022). Those galaxies with a velocity difference less than 2500 km s^{-1} from the BCGs are taken as true member galaxies. The member galaxy candidates of clusters determined by photometric redshifts only are cross-matched with the spectroscopic data of the GAMA. We find that 78% of the member galaxy candidates can be verified by spectroscopic redshift if the BCGs are not included, or up to 83% if BCGs are included. As seen in Figure 8, more massive galaxies have a higher fraction of true members detected. Due to the uncertainty of photometric redshifts, some true members are not included in the redshift slices. The missing member galaxies are such galaxies with a velocity difference of less than 2500 km s^{-1} from the BCGs. The missing fraction is about 8% of true members, slightly higher for lower mass galaxies (see Figure 8). Note that the GAMA survey is much shallow compared to the DESI Legacy Surveys, this test is made only for the bright galaxies in the DESI Legacy Surveys.

The cluster richness λ_{500} is compared to the mass M_{500} for the common clusters in Wen & Han (2015). As shown in

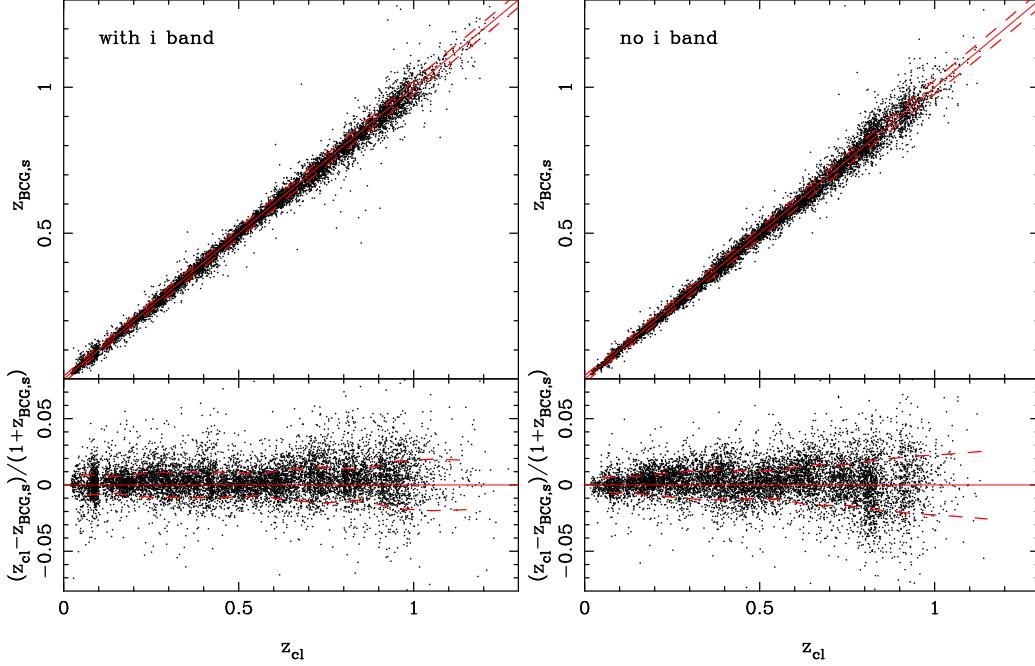


Figure 7. In the left panel, the comparison between photometric redshifts and spectroscopic redshifts for clusters identified with i band data. In every redshift interval of 0.1, 1000 clusters are randomly. The solid line is for equal values, and dashed lines represent the deviation of 1σ . The right panel is the same as the left, but for clusters identified without i band data in the shallowest region of Dec. $\geq 32^\circ$.

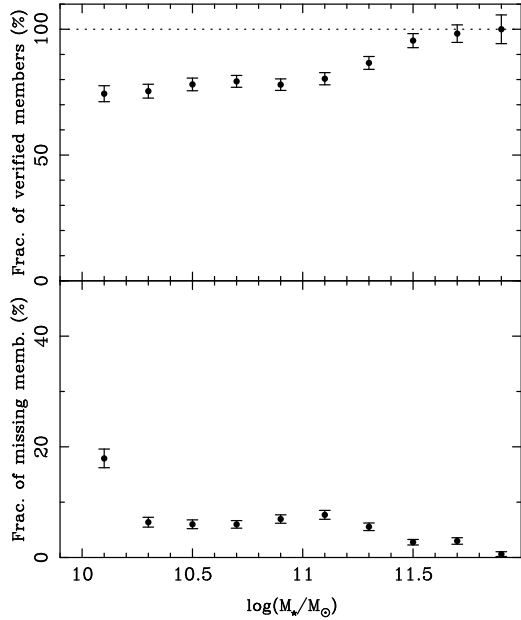


Figure 8. Verification of cluster members as a function of the stellar mass of galaxies by using the spectroscopic survey data of the GAMA (Driver et al. 2022). Upper panel: the fraction of verified member galaxies ($N_{\text{veri.}}/N_{\text{all}}$); Lower panel: the fraction of missed true member galaxies ($N_{\text{missing}}/N_{\text{real}}$). Here, $N_{\text{veri.}}$, N_{missing} , N_{real} are number of galaxies defined within a small spectroscopic redshift offset from the BCGs.

Figure 9, they are well correlated and can be scaled by

$$\log M_{500} = (0.97 \pm 0.03) \log \lambda_{500} - (1.30 \pm 0.02), \quad (4)$$

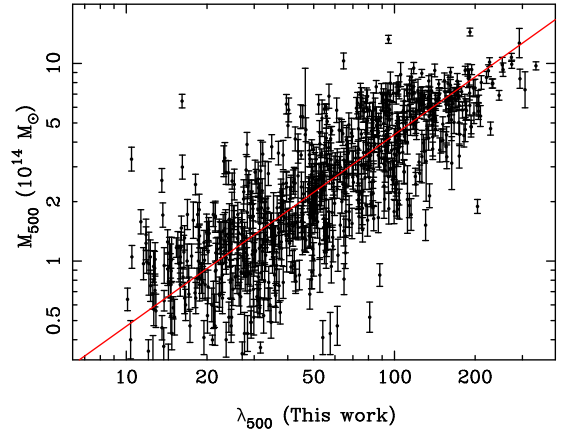


Figure 9. Correlation between cluster richness and cluster masses compiled in Wen & Han (2015). The solid is the best fit for the data.

where M_{500} is in unit of $10^{14} M_{\odot}$. The richness threshold of $\lambda_{500} = 10$ corresponds to the mass of $M_{500} \sim 0.47 \times 10^{14} M_{\odot}$. By the Equation 4, the M_{500} can be estimated by λ_{500} with an uncertainty of 0.20 dex for all identified clusters.

4. CROSS-MATCHING CLUSTERS WITH THOSE IN PREVIOUS CATALOGS

In the sky area of DESI Legacy Surveys, some survey data have previously been released, from which a large number of clusters of galaxies have been identified in the literature, as marked in the last column of Table 2.

In the following, we cross-match the identified clusters with those in some defined redshift ranges and sky regions in

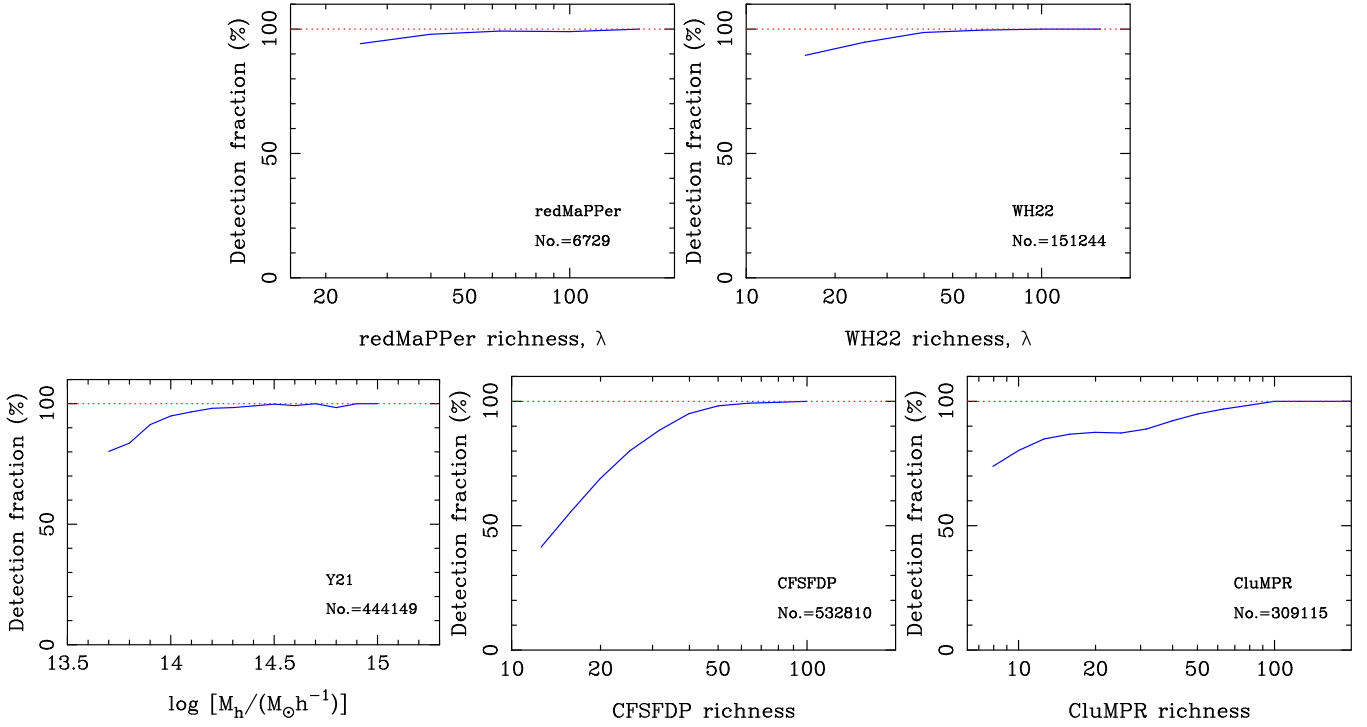


Figure 10. The detection fraction of clusters as a function of richness or halo mass for clusters in the redMaPPer (Rykoff et al. 2016), WH22 (Wen & Han 2022), Y21 (Yang et al. 2021), CFSFDP (Zou et al. 2022) and CluMPR (Yantovski-Barth et al. 2023) catalogs.

previous cluster catalogs, including the optical clusters from the DESI Legacy surveys and DES, the X-ray clusters from *ROSAT* All-Sky Survey (RASS) and extended ROentgen Survey with an Imaging Telescope Array (eROSITA), and the SZ clusters from Planck, South Pole Telescope (SPT) and Atacama Cosmology Telescope (ACT).

4.1. DES and DESI Legacy Surveys clusters

Rykoff et al. (2014) identified galaxy clusters based on the red-sequence feature of cluster galaxies, and presented the redMaPPer cluster catalog. The red sequence model was calibrated by using a training sample and then applied to photometric data to search clusters. From the DES Y1 data covering a sky area of ~ 1800 deg², 6729 redMaPPer clusters in the redshift range of $0.2 < z \lesssim 0.8$ were identified (Rykoff et al. 2016). Cross-matching with our clusters in the same sky region and the redshift range shows that 95% of redMaPPer clusters can be detected within a redshift difference of $0.05(1+z)$ and a projected distance of $1.5 r_{500}$ from our clusters. As shown in Figure 10, the detection fraction depends on richness, and near 100% clusters with a richness of $\lambda > 50$ are detected. Understandably some clusters with a small richness are missed due to the uncertainties of photometric redshifts of galaxies and hence the member recognition.

Wen & Han (2022, WH22) applied the same algorithm as in this paper to the DES data and identified 151,244 clusters at $0.1 < z < 1.5$. About 94% of clusters at $z < 1$ can be

found in the catalog of this work. The detection fraction is near 100% for rich clusters of $\lambda > 50$ (see Figure 10).

Three cluster samples obtained from photometric redshifts of the DESI Legacy Surveys DR9 have also been cross-matched with our catalog. Yang et al. (2021, Y21) used the friend-of-friend algorithm and identified 5.8 million groups in the redshift range of $z < 1$, which have at least three members⁴. Zou et al. (2022) applied “the clustering by Fast Search and Find of Density Peaks (CFSFDP)” algorithm and identified 532,810 clusters⁵ also in the redshift range of $z < 1$. Yantovski-Barth et al. (2023) presented “the Clusters from Masses and Photometric Redshifts (CluMPR)” algorithm and found 309,115 clusters⁶ in the redshift range of $0.1 < z < 1$. The Y21 catalog contains many galaxy groups down to a very low mass. We here choose the 444,149 clusters with the halo masses (M_h) above our threshold after the mass conversion function $M_{500} = 0.55 M_h$ (Hu & Kravtsov 2003) is applied. In our cluster catalog, we detect 92% of Y21 clusters, 72% of CFSFDP clusters and 86% of CluMPR clusters, respectively. The detection fractions vary as a function of cluster mass or richness.

Noticed that some clusters in previous catalogs are not detected by our algorithm. We investigate and find three rea-

⁴ <https://gax.sjtu.edu.cn/data/DESI.html>

⁵ <https://www.doi.org/10.11922/sciencedb.o00069.00003>

⁶ <https://zenodo.org/record/8157752>

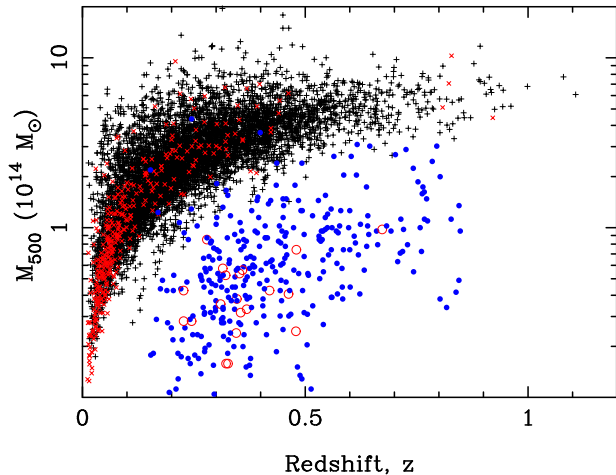


Figure 11. Mass–redshift diagram for clusters in RASS-MCMF (Klein et al. 2023) and eROSITA catalogs (Bulbul et al. 2022). The matched RASS-MCMF clusters are shown by plus and the unmatched ones by red crosses. The matched eROSITA clusters are shown by blue dots and the unmatched ones by red circles.

sons. The first is that a cluster is located in a cluster-binary system, probably just starting the merging process. We find both, but their small separation ($< 1.5 r_{500}$) leads us to regard them as one cluster. The poorer one is removed during our cleaning stage but are listed in the other catalogs with a different cluster center. Second, the unmatched clusters in previous catalogs have no BCG-like galaxies. The rest are clusters with BCG-like galaxies, but their richness and the total number of member galaxy candidates are below our thresholds.

4.2. X-ray clusters

The X-ray emission of galaxy clusters comes from the hot intracluster gas. Both the hot gas and galaxy components trace the mass distribution inside a cluster. In principle, any optical cluster should have a counterpart in X-ray. We cross-match our clusters from the DESI Legacy Surveys with the X-ray clusters identified from *ROSAT* All-Sky Survey (Klein et al. 2023) and eROSITA (Liu et al. 2022; Bulbul et al. 2022). We find that most *ROSAT* clusters are massive, while the eROSITA clusters are much less massive, as shown in Figure 11.

Klein et al. (2023) presented a large X-ray cluster sample based on joint analysis of the second RASS source catalog (2RXS) and the DESI Legacy Surveys data. They searched for optical counterparts of 2RXS sources by using a multi-component matched filter (MCMF) algorithm (Klein et al. 2018). The redshift, optical richness, and X-ray luminosity are derived, and a probability of being a random superposition f_{cont} is given. The RASS-MCMF catalog contains 8449 X-ray clusters at $z < 1$ with a purity of 90%. In the sky coverage of this work, there are 7898 RASS-MCMF clus-

ters. We find that 90% of them are detected in this paper. The matched and unmatched RASS-MCMF clusters are shown in the mass–redshift diagram in Figure 11. The detection fractions increase to 93% and 95% for the RASS-MCMF subsamples with the purities of 95% and 99%, respectively.

The eROSITA all-sky survey is 25 times more sensitive than the RASS, and it aims to detect about 50,000–100,000 galaxy clusters (Merloni et al. 2012). The data release of the eROSITA Final Equatorial-Depth Survey (eFEDS) covers an area of $\sim 140 \text{ deg}^2$. Liu et al. (2022) detected 542 candidates of galaxy clusters and groups at $0.01 < z < 1.3$ with an extended X-ray morphology. The sample has the completeness of 40% and the purity of 80% down to the flux limit of $10^{-14} \text{ erg s}^{-1} \text{ cm}^{-2}$. We take a subsample of 262 clusters and groups with an extent likelihood ≥ 15 , that has a purity of 90%. We find that 91% eROSITA clusters and groups are detected in this work. The X-ray candidates of galaxy clusters and groups with a smaller extent likelihood probably may easily be misclassified from point sources. Another eFEDS cluster catalog contains 346 galaxy clusters and groups in the redshift range of $0.1 < z < 1.3$ with a mass of $> 10^{13} M_{\odot}$ (Bulbul et al. 2022), of which 92% clusters and groups can be found in our sample (see Figure 11). After our paper has been submitted, the first eROSITA All-Sky Survey (eRASS1) published the largest X-ray cluster catalog, which contains 12,247 clusters in the western Galactic hemisphere (Bulbul et al. 2024), with a purity of 86%. About 82% eRASS1 clusters have been detected in our sample. The cross-matching indicates that our optical sample has a good completeness, even for low mass clusters of about $5 \times 10^{13} M_{\odot}$.

We check the data and also visually inspect the color images of the DESI Legacy Surveys to investigate why some X-ray clusters are missing in our cluster catalog. We find that some of them are merging clusters, with a projected distance between the optical and X-ray positions larger than the matching radius. Otherwise, the BCGs in some clusters are not found due to the cut-off caused by photometry flags. For most of the low-mass clusters, we can see the overdensity of member galaxy candidates but the BCG stellar mass or the richness estimated from member galaxy candidates is lower than our thresholds.

4.3. SZ clusters

The SZ effect is the result of inverse Compton scattering of cosmic microwave background by the hot intracluster gas. The surface brightness of the SZ effect is independent of redshift, so that detecting massive clusters via the SZ effect has the advantage to get clusters at high redshifts (Carlstrom et al. 2002).

The *Planck* satellite carried out an all-sky millimeter survey in the millimeter bands (Planck Collaboration et al.

2014). The second release of the *Planck* SZ catalog contains 1653 massive clusters with $M_{500} > 2 \times 10^{14} M_{\odot}$ (Planck Collaboration et al. 2016), of which 789 clusters are located in the DESI Legacy Surveys footprint. We find 746 matched clusters in a redshift difference of $0.05(1+z)$, giving the detection rate of at least 99%. A careful check shows that another 35 Planck clusters have a poor redshift estimate and can be matched within a larger redshift difference (Wen & Han 2022). One undetected cluster has the total number of galaxy candidates of $N_{\text{gal}} = 5$, below our threshold. We inspect the color images of the other seven clusters, and find no BCG-like galaxies and no overdensity of member galaxy candidates in the given redshift slice. They are probably false detections of the SZ clusters.

The ACT has detected galaxy clusters at the frequencies of 148 GHz, 218 GHz and 227 GHz with an angular resolution of 1.4 arcmin at 148 GHz (Swetz et al. 2011). The latest ACT SZ catalog includes 4195 massive clusters of $M_{500} > 1.5 \times 10^{14} M_{\odot}$ at redshifts $0.04 < z < 1.95$ from a sky area of $13,211 \text{ deg}^2$ (Hilton et al. 2021), of which 3914 clusters are located in the DESI Legacy Surveys sky area. The SPT is another excellent facility for detecting SZ clusters at the frequencies of 95, 150 and 220 GHz (Bleem et al. 2015). The SPT cluster catalog contains 1442 massive clusters up to redshift ~ 1.6 from three surveys with different regions and depths (Bleem et al. 2015, 2020; Huang et al. 2020; Bleem et al. 2023). We detect 95% ACT clusters and 93% SPT clusters in our optical cluster sample. The other non-detected clusters are mostly at high redshifts of $z > 1$.

5. EVOLUTION OF DYNAMICAL STATES OF CLUSTERS AND BCGS

Following Wen & Han (2013), we assess the dynamical states of rich clusters by using the cluster substructures shown by member galaxy distribution. In addition, we discuss the growth of BCG stellar masses with redshift.

5.1. Dynamical states of clusters

Dynamical states are fundamental for many studies of galaxy clusters because they contain the information on the assembly history of clusters (Smith & Taylor 2008). The dynamical parameters affect the mass determination of clusters in cosmological studies (Smith et al. 2003), and constrain astrophysics processes inside clusters, e.g. gas cooling, heating, and electron acceleration (Burns et al. 2008; Feretti et al. 2012). Clusters have various dynamic states, and are often classified simply as relaxed clusters and unrelaxed clusters. About 30%–80% clusters show significant substructures in optical or X-ray, and they are in unrelaxed states (e.g. Dressler & Shectman 1988; Santos et al. 2008; De Luca et al. 2021). It has been suggested that dynamical states and substructures significantly evolve with

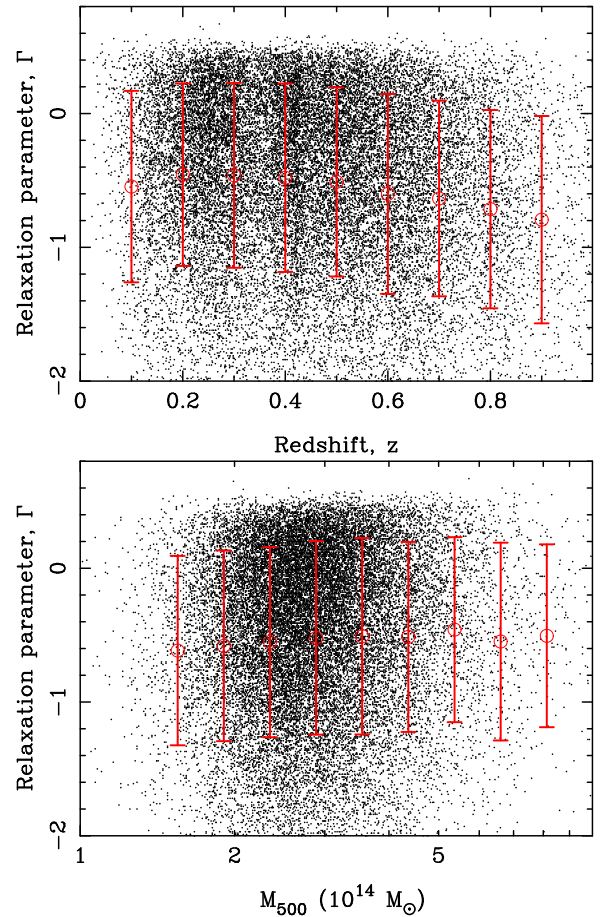


Figure 12. The distribution of relaxation parameter Γ for 28,038 massive clusters, indicating no significant evolution with redshift (upper panel) and non-dependence with cluster mass (lower panel). The open circles and the error bars represent the mean value and scatter of dataset, respectively.

redshift (e.g. Maughan et al. 2008; Mann & Ebeling 2012), but not conclusive (e.g. Weißmann et al. 2013; Wen & Han 2013; Ghirardini et al. 2022), mainly due to the criteria for relaxed clusters and the bias of selected sample (Eckert et al. 2011).

Wen & Han (2013) presented a method to measure dynamical states of galaxy clusters based on optical photometric data. First, a smoothed optical map is obtained from the 2-dimensional distribution of member galaxies weighting their luminosities. Then, three quantities are calculated: the asymmetry, the ridge flatness, and the normalized deviation of the smoothed map within the region of r_{500} . The asymmetry measures the asymmetry of the distribution of smoothed optical light around the cluster center. The ridge flatness measures the relative steepness of the ridge direction with the most flat light profile to the other directions. The normalized deviation measures the deviation of the optical map to a model. After testing a cluster sample, three measurements are combined to define a relaxation parameter, Γ , which has

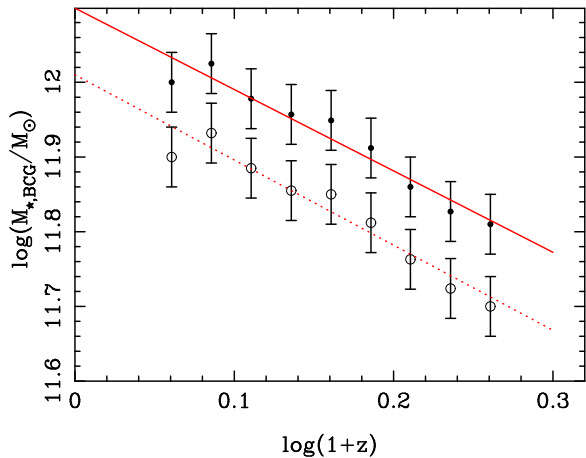


Figure 13. To keep a constant comoving number density of BCGs, the stellar mass threshold of BCGs as a function of redshift. The dots and open circles represent the thresholds starting from a reference value of $M_{*,\text{BCG}} = 10^{12} M_{\odot}$ and $10^{11.9} M_{\odot}$ at $z = 0.1 - 0.2$, respectively. The solid and dashed lines are the best fits the data in dots and open circles, respectively.

been used to quantify the dynamical states of a sample of 2092 rich clusters. This relaxation parameter is well correlated with the dynamical parameters obtained from X-ray measurements (Wen & Han 2013; Yuan & Han 2020).

For 28,038 rich clusters in our catalog which have more than 30 member galaxy candidates, we calculate their Γ values as listed in Table 2. This is the largest sample of optical clusters with dynamical state quantified. The distribution of Γ values is shown in Figure 12. Dynamical states of clusters have a wide distribution of Γ values, not a bimodal distribution for relaxed and unrelaxed states. No significant variation of Γ with redshift or cluster mass is found, consistent with the conclusions we previously obtained from the SDSS clusters (Wen & Han 2013) and Nurgaliev et al. (2017) obtained from a X-ray cluster sample.

If relaxed and unrelaxed clusters have to be divided literally by separating them at $\Gamma = 0$, one can get 26.5% of rich clusters identified in this paper being dynamically relaxed, which is consistent with 28% for the rich SDSS clusters by Wen & Han (2013).

5.2. Growth of BCGs

The BCGs have intriguing properties, and their evolution is tightly related to the host clusters (Von Der Linden et al. 2007; Wen et al. 2012; Yuan & Wen 2022). The stellar mass of BCGs can be a good tracer to understand their evolution. From simulations by De Lucia & Blaizot (2007), the BCG stellar mass grows by a factor of 3 from $z = 1$ to $z = 0$. Diverse results were later obtained by observations (e.g. Lin et al. 2013; Zhang et al. 2016; Wen & Han 2021). The infrared luminosities were found to be consistent with a passive evolution model since $z \sim 1$, suggesting no signif-

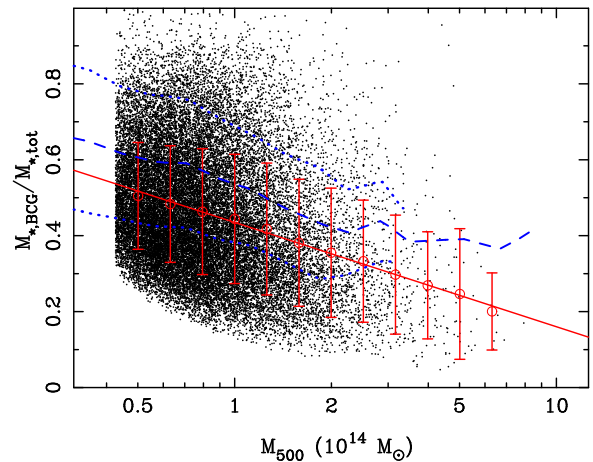


Figure 14. The fraction for BCG stellar mass of total stellar mass of galaxies in clusters, plotted as a function of cluster mass. The average and data dispersions are given by circles and error-bar, with a fitted line. The dashed line and dotted line come from the simulations by (Kravtsov et al. 2018) for the mean fraction and the dispersion.

icant change in the BCG stellar masses (Whiley et al. 2008; Stott et al. 2010). Lidman et al. (2012) corrected the relation between BCG stellar mass and cluster mass, and found that the stellar mass of BCGs increases by a factor of 1.8 ± 0.3 from $z = 0.9$ to 0.2 .

Here, we investigate the growth of the BCG stellar mass by a new approach. Assuming that the merger between BCGs is negligible, the comoving number density of BCGs should be a constant over cosmic time for a volume-limited complete sample. Since all BCGs in our large cluster sample have a mass $M_{*,\text{BCG}} > 10^{11} M_{\odot}$, we can take a high threshold of BCG stellar mass for clusters in the redshift range of $z = 0.1 - 0.2$ as the reference, and then reduce the threshold of BCG stellar mass to keep the same comoving density of BCGs in other redshift bins, as shown by Figure 13. For BCGs with a threshold of BCG stellar mass $M_{*,\text{BCG}} > 10^{12} M_{\odot}$ in the redshift range of $z = 0.1 - 0.2$, the thresholds in other redshift bins can be fitted by a linear law in the log-log space,

$$\log(M_{*,\text{BCG}}) = (12.10 \pm 0.02) - (1.09 \pm 0.10) \log(1+z). \quad (5)$$

This relation implies that the stellar mass grows by a factor of $2.12^{+0.16}_{-0.14}$ since $z = 1$. If a threshold of $M_{*,\text{BCG}} = 10^{11.9} M_{\odot}$ is chosen, one can get fit to the thresholds by

$$\log(M_{*,\text{BCG}}) = (12.01 \pm 0.02) - (1.14 \pm 0.11) \log(1+z), \quad (6)$$

which means that the stellar masses of BCGs grow by a factor of $2.20^{+0.17}_{-0.16}$ since $z = 1$. Our results are consistent with previous works based on observation data (Lidman et al. 2012; Zhang et al. 2016; Wen & Han 2021).

In optical, the BCG is usually dominant inside a cluster. The dominance of BCGs in clusters can be expressed by the fraction of BCG stellar mass relative to the total stellar mass (including the BCG) if the members of clusters are highly complete. We therefore take all clusters at $z < 0.5$ for this work. As seen in Figure 14, the fraction of BCG stellar mass decreases with cluster mass, indicating the BCGs are less dominant in more massive clusters with more member galaxies, consistent with the results from simulations (Kravtsov et al. 2018). The mean fraction depends on cluster mass by the relation

$$\frac{M_{*,\text{BCG}}}{M_{*,\text{tot}}} = (0.435 \pm 0.003) - (0.275 \pm 0.007) \log M_{500}. \quad (7)$$

In addition, we investigate how many BCG-like galaxies are located in the clusters. BCG-like galaxies are considered as being cluster members if they have a projected separation within $1.5 r_{500}$ and a redshift difference less than Δ_z . We find that about 76% of massive galaxies with a mass of $M_* \sim 10^{12} M_\odot$, or about 50% of galaxies of $M_* \sim 10^{11.7} M_\odot$ or 10% at $M_* \sim 10^{11} M_\odot$, are located in the identified clusters. Therefore, finding out massive BCG-like galaxies is a useful first step to identifying galaxy clusters.

6. SUMMARY

By using photometric redshifts and available spectroscopic redshifts of galaxies in the joint DESI Legacy Surveys and WISE data, we obtain a large catalog of 1.58 million galaxy clusters and investigate their properties.

We first estimate the photometric redshifts for 295.6 million galaxies in the latest released data in the *grizW1W2* bands by using the nearest-neighbor algorithm. The redshift uncertainty is about 0.013 for bright galaxies of $z_m < 21$ and increases to 0.053 for faint galaxies of $z_m > 22$. The stellar mass is estimated from the *zW1*-band luminosities for galaxies in the DR10 and also those galaxies in the DR9 if their photometric redshifts are estimated.

Then, we identify a large sample of 1.58 million galaxy clusters based on the overdensity of total galaxy stellar mass within a redshift slice around BCG-like galaxies. Among them, 877,806 clusters are identified for the first time. The redshift distribution extends to $z < 1.5$, and 338,841 clusters have spectroscopic redshift. The uncertainty of cluster photometric redshift is about 0.010. The cluster richness has a good correlation with cluster mass, which indicates that the identified clusters have an equivalent mass of $M_{500} \geq 0.47 \times 10^{14} M_\odot$. Our cluster catalog includes most of the massive clusters in previous optical, X-ray and SZ cluster catalogs.

We assess the dynamical states for 28,038 rich clusters based on the substructures of the distribution of cluster member galaxies. No significant evolution of dynamical states is

shown. In addition, we find that the stellar mass of BCGs increases by a factor of 2 after $z = 1$. The fraction for the BCG stellar mass relative to the total stellar mass decreases with cluster mass, implying less dominance of BCGs in richer clusters.

ACKNOWLEDGMENTS

We thank the referee for the valuable comments that helped to improve the paper. The authors are partially supported by the National Natural Science Foundation of China (Grant Numbers 11988101, 11833009 and 12073036), the Key Research Program of the Chinese Academy of Sciences (Grant Number QYZDJ-SSW-SLH021). We also acknowledge the support of the science research grants from the China Manned Space Project with Numbers CMS-CSST-2021-A01 and CMS-CSST-2021-B01.

The Legacy Surveys consist of three individual and complementary projects: the Dark Energy Camera Legacy Survey (DECaLS; Proposal ID # 2014B-0404; PIs: David Schlegel and Arjun Dey), the Beijing-Arizona Sky Survey (BASS; NOAO Prop. ID # 2015A-0801; PIs: Zhou Xu and Xiaohui Fan), and the Mayall *z*-band Legacy Survey (MzLS; Prop. ID # 2016A-0453; PI: Arjun Dey). DECaLS, BASS, and MzLS together include data obtained, respectively, at the Blanco telescope, Cerro Tololo Inter-American Observatory, NSF's NOIRLab; the Bok telescope, Steward Observatory, University of Arizona; and the Mayall telescope, Kitt Peak National Observatory, NOIRLab. Pipeline processing and analyses of the data were supported by NOIRLab and the Lawrence Berkeley National Laboratory (LBNL). The Legacy Surveys project is honored to be permitted to conduct astronomical research on Iolkam Du'ag (Kitt Peak), a mountain with particular significance to the Tohono O'odham Nation.

NOIRLab is operated by the Association of Universities for Research in Astronomy (AURA) under a cooperative agreement with the National Science Foundation. LBNL is managed by the Regents of the University of California under contract to the U.S. Department of Energy.

This project used data obtained with the Dark Energy Camera (DECam), which was constructed by the Dark Energy Survey (DES) collaboration. Funding for the DES Projects has been provided by the U.S. Department of Energy, the U.S. National Science Foundation, the Ministry of Science and Education of Spain, the Science and Technology Facilities Council of the United Kingdom, the Higher Education Funding Council for England, the National Center for Supercomputing Applications at the University of Illinois at Urbana-Champaign, the Kavli Institute of Cosmological Physics at the University of Chicago, Center for Cosmology and Astro-Particle Physics at the Ohio State University, the Mitchell Institute for Fundamental Physics and

Astronomy at Texas A&M University, Financiadora de Estudos e Projetos, Fundacao Carlos Chagas Filho de Amparo, Financiadora de Estudos e Projetos, Fundacao Carlos Chagas Filho de Amparo a Pesquisa do Estado do Rio de Janeiro, Conselho Nacional de Desenvolvimento Cientifico e Tecnologico and the Ministerio da Ciencia, Tecnologia e Inovacao, the Deutsche Forschungsgemeinschaft and the Collaborating Institutions in the Dark Energy Survey. The Collaborating Institutions are Argonne National Laboratory, the University of California at Santa Cruz, the University of Cambridge, Centro de Investigaciones Energeticas, Medioambientales y Tecnologicas-Madrid, the University of Chicago, University College London, the DES-Brazil Consortium, the University of Edinburgh, the Eidgenossische Technische Hochschule (ETH) Zurich, Fermi National Accelerator Laboratory, the University of Illinois at Urbana-Champaign, the Institut de Ciencies de l’Espai (IEEC/CSIC), the Institut de Fisica d’Altes Energies, Lawrence Berkeley National Laboratory, the Ludwig Maximilians Universitat Munchen and the associated Excellence Cluster Universe, the University of Michigan, NSF’s NOIRLab, the University of Nottingham, the Ohio State University, the University of Pennsylvania, the University of Portsmouth, SLAC National Accelerator Laboratory, Stanford University, the University of Sussex, and Texas A&M University.

BASS is a key project of the Telescope Access Program (TAP), which has been funded by the National Astronomical Observatories of China, the Chinese Academy of Sciences (the Strategic Priority Research Program “The Emergence of Cosmological Structures” Grant # XDB09000000), and the Special Fund for Astronomy from the Ministry of Finance. The BASS is also supported by the External Cooperation Program of the Chinese Academy of Sciences (Grant # 114A11KYSB20160057), and Chinese National Natural Science Foundation (Grant # 12120101003, # 11433005). The Legacy Survey team makes use of data products from the Near-Earth Object Wide-field Infrared Survey Explorer (NEOWISE), which is a project of the Jet Propulsion Laboratory/California Institute of Technology. NEOWISE is funded by the National Aeronautics and Space Administration.

The Legacy Surveys imaging of the DESI footprint is supported by the Director, Office of Science, Office of High Energy Physics of the U.S. Department of Energy under Contract No. DE-AC02-05CH1123, by the National Energy Research Scientific Computing Center, a DOE Office of Science User Facility under the same contract; and by the U.S. National Science Foundation, Division of Astronomical Sciences under Contract No. AST-0950945 to NOAO.

The Photometric Redshifts for the Legacy Surveys (PRLS) catalog used in this paper was produced, thanks to funding from the U.S. Department of Energy Office of Science, Office of High Energy Physics via grant DE-SC0007914.

REFERENCES

- Abbott, T. M. C., Adamów, M., Aguena, M., et al. 2021, *ApJS*, 255, 20, doi: [10.3847/1538-4365/ac00b3](https://doi.org/10.3847/1538-4365/ac00b3)
- Abdurro’uf, Accetta, K., Aerts, C., et al. 2022, *ApJS*, 259, 35, doi: [10.3847/1538-4365/ac4414](https://doi.org/10.3847/1538-4365/ac4414)
- Abell, G. O. 1958, *ApJS*, 3, 211
- Abell, G. O., Corwin, Jr., H. G., & Olowin, R. P. 1989, *ApJS*, 70, 1, doi: [10.1086/191333](https://doi.org/10.1086/191333)
- Aguena, M., Benoist, C., da Costa, L. N., et al. 2021, *MNRAS*, 502, 4435, doi: [10.1093/mnras/stab264](https://doi.org/10.1093/mnras/stab264)
- Allen, S. W., Evrard, A. E., & Mantz, A. B. 2011, *ARA&A*, 49, 409, doi: [10.1146/annurev-astro-081710-102514](https://doi.org/10.1146/annurev-astro-081710-102514)
- Andreon, S. 2010, *MNRAS*, 407, 263, doi: [10.1111/j.1365-2966.2010.16856.x](https://doi.org/10.1111/j.1365-2966.2010.16856.x)
- Banerjee, A., Adhikari, S., Dalal, N., More, S., & Kravtsov, A. 2020, *JCAP*, 2020, 024, doi: [10.1088/1475-7516/2020/02/024](https://doi.org/10.1088/1475-7516/2020/02/024)
- Banerjee, P., Szabo, T., Pierpaoli, E., et al. 2018, *NewA*, 58, 61, doi: [10.1016/j.newast.2017.07.008](https://doi.org/10.1016/j.newast.2017.07.008)
- Bell, E. F., McIntosh, D. H., Katz, N., & Weinberg, M. D. 2003, *ApJS*, 149, 289, doi: [10.1086/378847](https://doi.org/10.1086/378847)
- Bleem, L. E., Stalder, B., de Haan, T., et al. 2015, *ApJS*, 216, 27, doi: [10.1088/0067-0049/216/2/27](https://doi.org/10.1088/0067-0049/216/2/27)
- Bleem, L. E., Bocquet, S., Stalder, B., et al. 2020, *ApJS*, 247, 25, doi: [10.3847/1538-4365/ab6993](https://doi.org/10.3847/1538-4365/ab6993)
- Bleem, L. E., Klein, M., Abbott, T. M. C., et al. 2023, arXiv e-prints, arXiv:2311.07512, doi: [10.48550/arXiv.2311.07512](https://doi.org/10.48550/arXiv.2311.07512)
- Böhringer, H., Chon, G., & Collins, C. A. 2014, *A&A*, 570, A31, doi: [10.1051/0004-6361/201323155](https://doi.org/10.1051/0004-6361/201323155)
- Bulbul, E., Liu, A., Pasini, T., et al. 2022, *A&A*, 661, A10, doi: [10.1051/0004-6361/202142460](https://doi.org/10.1051/0004-6361/202142460)
- Bulbul, E., Liu, A., Kluge, M., et al. 2024, arXiv e-prints, arXiv:2402.08452, doi: [10.48550/arXiv.2402.08452](https://doi.org/10.48550/arXiv.2402.08452)
- Burns, J. O., Hallman, E. J., Gantner, B., Motl, P. M., & Norman, M. L. 2008, *ApJ*, 675, 1125, doi: [10.1086/526514](https://doi.org/10.1086/526514)
- Carlstrom, J. E., Holder, G. P., & Reese, E. D. 2002, *ARA&A*, 40, 643, doi: [10.1146/annurev.astro.40.060401.093803](https://doi.org/10.1146/annurev.astro.40.060401.093803)
- Cavaliere, A., & Fusco-Femiano, R. 1976, *A&A*, 49, 137
- Civano, F., Marchesi, S., Comastri, A., et al. 2016, *ApJ*, 819, 62, doi: [10.3847/0004-637X/819/1/62](https://doi.org/10.3847/0004-637X/819/1/62)
- Darvish, B., Mobasher, B., Martin, D. C., et al. 2017, *ApJ*, 837, 16, doi: [10.3847/1538-4357/837/1/16](https://doi.org/10.3847/1538-4357/837/1/16)
- De Luca, F., De Petris, M., Yepes, G., et al. 2021, *MNRAS*, 504, 5383, doi: [10.1093/mnras/stab1073](https://doi.org/10.1093/mnras/stab1073)

- De Lucia, G., & Blaizot, J. 2007, *MNRAS*, 375, 2, doi: [10.1111/j.1365-2966.2006.11287.x](https://doi.org/10.1111/j.1365-2966.2006.11287.x)
- DESI Collaboration, Adame, A. G., Aguilar, J., et al. 2023, arXiv e-prints, arXiv:2306.06308, doi: [10.48550/arXiv.2306.06308](https://doi.org/10.48550/arXiv.2306.06308)
- Dey, A., Schlegel, D. J., Lang, D., et al. 2019, *AJ*, 157, 168, doi: [10.3847/1538-3881/ab089d](https://doi.org/10.3847/1538-3881/ab089d)
- Dressler, A., & Shectman, S. A. 1988, *AJ*, 95, 985, doi: [10.1086/114694](https://doi.org/10.1086/114694)
- Driver, S. P., Bellstedt, S., Robotham, A. S. G., et al. 2022, *MNRAS*, 513, 439, doi: [10.1093/mnras/stac472](https://doi.org/10.1093/mnras/stac472)
- Drlica-Wagner, A., Ferguson, P. S., Adamów, M., et al. 2022, *ApJS*, 261, 38, doi: [10.3847/1538-4365/ac78eb](https://doi.org/10.3847/1538-4365/ac78eb)
- Eckert, D., Molendi, S., & Paltani, S. 2011, *A&A*, 526, A79, doi: [10.1051/0004-6361/201015856](https://doi.org/10.1051/0004-6361/201015856)
- Feretti, L., Giovannini, G., Govoni, F., & Murgia, M. 2012, *A&A Rv*, 20, 54, doi: [10.1007/s00159-012-0054-z](https://doi.org/10.1007/s00159-012-0054-z)
- Gal, R. R., de Carvalho, R. R., Lopes, P. A. A., et al. 2003, *AJ*, 125, 2064, doi: [10.1086/368240](https://doi.org/10.1086/368240)
- Ghirardini, V., Bahar, Y. E., Bulbul, E., et al. 2022, *A&A*, 661, A12, doi: [10.1051/0004-6361/202141639](https://doi.org/10.1051/0004-6361/202141639)
- Gozaliasl, G., Finoguenov, A., Tanaka, M., et al. 2019, *MNRAS*, 483, 3545, doi: [10.1093/mnras/sty3203](https://doi.org/10.1093/mnras/sty3203)
- Hansen, S. M., Sheldon, E. S., Wechsler, R. H., & Koester, B. P. 2009, *ApJ*, 699, 1333, doi: [10.1088/0004-637X/699/2/1333](https://doi.org/10.1088/0004-637X/699/2/1333)
- Hao, J., McKay, T. A., Koester, B. P., et al. 2010, *ApJS*, 191, 254, doi: [10.1088/0067-0049/191/2/254](https://doi.org/10.1088/0067-0049/191/2/254)
- Hasinger, G., Cappelluti, N., Brunner, H., et al. 2007, *ApJS*, 172, 29, doi: [10.1086/516576](https://doi.org/10.1086/516576)
- Hilton, M., Sifón, C., Naess, S., et al. 2021, *ApJS*, 253, 3, doi: [10.3847/1538-4365/abd023](https://doi.org/10.3847/1538-4365/abd023)
- Hong, T., Han, J. L., & Wen, Z. L. 2016, *ApJ*, 826, 154, doi: [10.3847/0004-637X/826/2/154](https://doi.org/10.3847/0004-637X/826/2/154)
- Hu, W., & Kravtsov, A. V. 2003, *ApJ*, 584, 702, doi: [10.1086/345846](https://doi.org/10.1086/345846)
- Huang, N., Bleem, L. E., Stalder, B., et al. 2020, *AJ*, 159, 110, doi: [10.3847/1538-3881/ab6a96](https://doi.org/10.3847/1538-3881/ab6a96)
- Huchra, J. P., Maeri, L. M., Masters, K. L., et al. 2012, *ApJS*, 199, 26, doi: [10.1088/0067-0049/199/2/26](https://doi.org/10.1088/0067-0049/199/2/26)
- Kauffmann, G., Heckman, T. M., White, S. D. M., et al. 2003, *MNRAS*, 341, 33, doi: [10.1046/j.1365-8711.2003.06291.x](https://doi.org/10.1046/j.1365-8711.2003.06291.x)
- Klein, M., Hernández-Lang, D., Mohr, J. J., Bocquet, S., & Singh, A. 2023, *MNRAS*, doi: [10.1093/mnras/stad2729](https://doi.org/10.1093/mnras/stad2729)
- Klein, M., Mohr, J. J., Desai, S., et al. 2018, *MNRAS*, 474, 3324, doi: [10.1093/mnras/stx2929](https://doi.org/10.1093/mnras/stx2929)
- Knobel, C., Lilly, S. J., Iovino, A., et al. 2012, *ApJ*, 753, 121, doi: [10.1088/0004-637X/753/2/121](https://doi.org/10.1088/0004-637X/753/2/121)
- Koester, B. P., McKay, T. A., Annis, J., et al. 2007, *ApJ*, 660, 239, doi: [10.1086/509599](https://doi.org/10.1086/509599)
- Kravtsov, A. V., Vikhlinin, A. A., & Meshcheryakov, A. V. 2018, *Astronomy Letters*, 44, 8, doi: [10.1134/S1063773717120015](https://doi.org/10.1134/S1063773717120015)
- Laigle, C., McCracken, H. J., Ilbert, O., et al. 2016, *ApJS*, 224, 24, doi: [10.3847/0067-0049/224/2/24](https://doi.org/10.3847/0067-0049/224/2/24)
- Lang, D. 2014, *AJ*, 147, 108, doi: [10.1088/0004-6256/147/5/108](https://doi.org/10.1088/0004-6256/147/5/108)
- Lauer, T. R., Postman, M., Strauss, M. A., Graves, G. J., & Chisari, N. E. 2014, *ApJ*, 797, 82, doi: [10.1088/0004-637X/797/2/82](https://doi.org/10.1088/0004-637X/797/2/82)
- Lidman, C., Suherli, J., Muzzin, A., et al. 2012, *MNRAS*, 427, 550, doi: [10.1111/j.1365-2966.2012.21984.x](https://doi.org/10.1111/j.1365-2966.2012.21984.x)
- Lin, Y.-T., Brodwin, M., Gonzalez, A. H., et al. 2013, *ApJ*, 771, 61, doi: [10.1088/0004-637X/771/1/61](https://doi.org/10.1088/0004-637X/771/1/61)
- Liske, J., Baldry, I. K., Driver, S. P., et al. 2015, *MNRAS*, 452, 2087, doi: [10.1093/mnras/stv1436](https://doi.org/10.1093/mnras/stv1436)
- Liu, A., Bulbul, E., Ghirardini, V., et al. 2022, *A&A*, 661, A2, doi: [10.1051/0004-6361/202141120](https://doi.org/10.1051/0004-6361/202141120)
- Liu, F. S., Mao, S., & Meng, X. M. 2012, *MNRAS*, 423, 422, doi: [10.1111/j.1365-2966.2012.20886.x](https://doi.org/10.1111/j.1365-2966.2012.20886.x)
- Liu, F. S., Xia, X. Y., Mao, S., Wu, H., & Deng, Z. G. 2008, *MNRAS*, 385, 23, doi: [10.1111/j.1365-2966.2007.12818.x](https://doi.org/10.1111/j.1365-2966.2007.12818.x)
- Lopes, P. A. A., de Carvalho, R. R., Gal, R. R., et al. 2004, *AJ*, 128, 1017, doi: [10.1086/423038](https://doi.org/10.1086/423038)
- Mann, A. W., & Ebeling, H. 2012, *MNRAS*, 420, 2120, doi: [10.1111/j.1365-2966.2011.20170.x](https://doi.org/10.1111/j.1365-2966.2011.20170.x)
- Markevitch, M., Gonzalez, A. H., Clowe, D., et al. 2004, *ApJ*, 606, 819, doi: [10.1086/383178](https://doi.org/10.1086/383178)
- Matthews, D. J., Newman, J. A., Coil, A. L., Cooper, M. C., & Gwyn, S. D. J. 2013, *ApJS*, 204, 21, doi: [10.1088/0067-0049/204/2/21](https://doi.org/10.1088/0067-0049/204/2/21)
- Maughan, B. J., Jones, C., Forman, W., & Van Speybroeck, L. 2008, *ApJS*, 174, 117, doi: [10.1086/521225](https://doi.org/10.1086/521225)
- McDonald, M., Stalder, B., Bayliss, M., et al. 2016, *ApJ*, 817, 86, doi: [10.3847/0004-637X/817/2/86](https://doi.org/10.3847/0004-637X/817/2/86)
- Merloni, A., Predehl, P., Becker, W., et al. 2012, arXiv e-prints, arXiv:1209.3114, doi: [10.48550/arXiv.1209.3114](https://doi.org/10.48550/arXiv.1209.3114)
- Nurgaliev, D., McDonald, M., Benson, B. A., et al. 2017, *ApJ*, 841, 5, doi: [10.3847/1538-4357/aa6db4](https://doi.org/10.3847/1538-4357/aa6db4)
- O'Dea, C. P., Baum, S. A., Privon, G., et al. 2008, *ApJ*, 681, 1035, doi: [10.1086/588212](https://doi.org/10.1086/588212)
- Oguri, M. 2014, *MNRAS*, 444, 147, doi: [10.1093/mnras/stu1446](https://doi.org/10.1093/mnras/stu1446)
- Oguri, M., Lin, Y.-T., Lin, S.-C., et al. 2018, *PASJ*, 70, S20, doi: [10.1093/pasj/psx042](https://doi.org/10.1093/pasj/psx042)
- Palmese, A., Annis, J., Burgad, J., et al. 2020, *MNRAS*, 493, 4591, doi: [10.1093/mnras/staa526](https://doi.org/10.1093/mnras/staa526)
- Pillepich, A., Nelson, D., Hernquist, L., et al. 2018, *MNRAS*, 475, 648, doi: [10.1093/mnras/stx3112](https://doi.org/10.1093/mnras/stx3112)
- Planck Collaboration, Ade, P. A. R., Aghanim, N., et al. 2014, *A&A*, 571, A1, doi: [10.1051/0004-6361/201321529](https://doi.org/10.1051/0004-6361/201321529)
- , 2016, *A&A*, 594, A27, doi: [10.1051/0004-6361/201525823](https://doi.org/10.1051/0004-6361/201525823)
- Rosati, P., Borgani, S., & Norman, C. 2002, *ARA&A*, 40, 539, doi: [10.1146/annurev.astro.40.120401.150547](https://doi.org/10.1146/annurev.astro.40.120401.150547)
- Rykoff, E. S., Rozo, E., Busha, M. T., et al. 2014, *ApJ*, 785, 104, doi: [10.1088/0004-637X/785/2/104](https://doi.org/10.1088/0004-637X/785/2/104)

- Rykoff, E. S., Rozo, E., Hollowood, D., et al. 2016, *ApJS*, 224, 1, doi: [10.3847/0067-0049/224/1/1](https://doi.org/10.3847/0067-0049/224/1/1)
- Sanders, D. B., Salvato, M., Aussel, H., et al. 2007, *ApJS*, 172, 86, doi: [10.1086/517885](https://doi.org/10.1086/517885)
- Santos, J. S., Rosati, P., Tozzi, P., et al. 2008, *A&A*, 483, 35, doi: [10.1051/0004-6361/20078815](https://doi.org/10.1051/0004-6361/20078815)
- Schlafly, E. F., Meisner, A. M., & Green, G. M. 2019, *ApJS*, 240, 30, doi: [10.3847/1538-4365/aafbea](https://doi.org/10.3847/1538-4365/aafbea)
- Scodreggio, M., Guzzo, L., Garilli, B., et al. 2018, *A&A*, 609, A84, doi: [10.1051/0004-6361/201630114](https://doi.org/10.1051/0004-6361/201630114)
- Scoville, N., Abraham, R. G., Aussel, H., et al. 2007, *ApJS*, 172, 38, doi: [10.1086/516580](https://doi.org/10.1086/516580)
- Smith, G. P., Edge, A. C., Eke, V. R., et al. 2003, *ApJL*, 590, L79, doi: [10.1086/376747](https://doi.org/10.1086/376747)
- Smith, G. P., & Taylor, J. E. 2008, *ApJL*, 682, L73, doi: [10.1086/591271](https://doi.org/10.1086/591271)
- Söchting, I. K., Coldwell, G. V., Clowes, R. G., Campusano, L. E., & Graham, M. J. 2012, *MNRAS*, 423, 2436, doi: [10.1111/j.1365-2966.2012.21050.x](https://doi.org/10.1111/j.1365-2966.2012.21050.x)
- Stott, J. P., Collins, C. A., Sahlén, M., et al. 2010, *ApJ*, 718, 23, doi: [10.1088/0004-637X/718/1/23](https://doi.org/10.1088/0004-637X/718/1/23)
- Sunyaev, R. A., & Zeldovich, Y. B. 1972, *Comments on Astrophysics and Space Physics*, 4, 173
- Swetz, D. S., Ade, P. A. R., Amiri, M., et al. 2011, *ApJS*, 194, 41, doi: [10.1088/0067-0049/194/2/41](https://doi.org/10.1088/0067-0049/194/2/41)
- Szabo, T., Pierpaoli, E., Dong, F., Pipino, A., & Gunn, J. 2011, *ApJ*, 736, 21, doi: [10.1088/0004-637X/736/1/21](https://doi.org/10.1088/0004-637X/736/1/21)
- Taniguchi, Y., Scoville, N., Murayama, T., et al. 2007, *ApJS*, 172, 9, doi: [10.1086/516596](https://doi.org/10.1086/516596)
- Thongkham, K., Gonzalez, A. H., Brodwin, M., et al. 2024, *arXiv e-prints*, arXiv:2403.16976, doi: [10.48550/arXiv.2403.16976](https://doi.org/10.48550/arXiv.2403.16976)
- Vikhlinin, A., Burenin, R. A., Ebeling, H., et al. 2009, *ApJ*, 692, 1033, doi: [10.1088/0004-637X/692/2/1033](https://doi.org/10.1088/0004-637X/692/2/1033)
- Von Der Linden, A., Best, P. N., Kauffmann, G., & White, S. D. M. 2007, *MNRAS*, 379, 867, doi: [10.1111/j.1365-2966.2007.11940.x](https://doi.org/10.1111/j.1365-2966.2007.11940.x)
- Weißmann, A., Böhringer, H., & Chon, G. 2013, *A&A*, 555, A147, doi: [10.1051/0004-6361/201321495](https://doi.org/10.1051/0004-6361/201321495)
- Wen, X.-Q., Wu, H., Zhu, Y.-N., et al. 2013, *MNRAS*, 433, 2946, doi: [10.1093/mnras/stt939](https://doi.org/10.1093/mnras/stt939)
- Wen, Z. L., & Han, J. L. 2011, *ApJ*, 734, 68, doi: [10.1088/0004-637X/734/1/68](https://doi.org/10.1088/0004-637X/734/1/68)
- , 2013, *MNRAS*, 436, 275, doi: [10.1093/mnras/stt1581](https://doi.org/10.1093/mnras/stt1581)
- , 2015, *ApJ*, 807, 178, doi: [10.1088/0004-637X/807/2/178](https://doi.org/10.1088/0004-637X/807/2/178)
- , 2021, *MNRAS*, 500, 1003, doi: [10.1093/mnras/staa3308](https://doi.org/10.1093/mnras/staa3308)
- , 2022, *MNRAS*, 513, 3946, doi: [10.1093/mnras/stac1149](https://doi.org/10.1093/mnras/stac1149)
- Wen, Z. L., Han, J. L., & Liu, F. S. 2009, *ApJS*, 183, 197, doi: [10.1088/0067-0049/183/2/197](https://doi.org/10.1088/0067-0049/183/2/197)
- , 2012, *ApJS*, 199, 34, doi: [10.1088/0067-0049/199/2/34](https://doi.org/10.1088/0067-0049/199/2/34)
- Wen, Z. L., Han, J. L., & Yang, F. 2018, *MNRAS*, 475, 343, doi: [10.1093/mnras/stx3189](https://doi.org/10.1093/mnras/stx3189)
- Wetzell, A. R., Tinker, J. L., & Conroy, C. 2012, *MNRAS*, 424, 232, doi: [10.1111/j.1365-2966.2012.21188.x](https://doi.org/10.1111/j.1365-2966.2012.21188.x)
- Whiley, I. M., Aragón-Salamanca, A., De Lucia, G., et al. 2008, *MNRAS*, 387, 1253, doi: [10.1111/j.1365-2966.2008.13324.x](https://doi.org/10.1111/j.1365-2966.2008.13324.x)
- Wright, E. L., Eisenhardt, P. R. M., Mainzer, A. K., et al. 2010, *AJ*, 140, 1868, doi: [10.1088/0004-6256/140/6/1868](https://doi.org/10.1088/0004-6256/140/6/1868)
- Yang, X., Xu, H., He, M., et al. 2021, *ApJ*, 909, 143, doi: [10.3847/1538-4357/abddb2](https://doi.org/10.3847/1538-4357/abddb2)
- Yantovski-Barth, M. J., Newman, J. A., Dey, B., et al. 2023, *arXiv e-prints*, arXiv:2307.10426, doi: [10.48550/arXiv.2307.10426](https://doi.org/10.48550/arXiv.2307.10426)
- Yuan, Z. S., & Han, J. L. 2020, *MNRAS*, 497, 5485, doi: [10.1093/mnras/staa2363](https://doi.org/10.1093/mnras/staa2363)
- Yuan, Z. S., & Wen, Z. L. 2022, *MNRAS*, 516, 3159, doi: [10.1093/mnras/stac2492](https://doi.org/10.1093/mnras/stac2492)
- Zamojski, M. A., Schiminovich, D., Rich, R. M., et al. 2007, *ApJS*, 172, 468, doi: [10.1086/516593](https://doi.org/10.1086/516593)
- Zhang, Y., Miller, C., McKay, T., et al. 2016, *ApJ*, 816, 98, doi: [10.3847/0004-637X/816/2/98](https://doi.org/10.3847/0004-637X/816/2/98)
- Zhou, R., Newman, J. A., Mao, Y.-Y., et al. 2021, *MNRAS*, 501, 3309, doi: [10.1093/mnras/staa3764](https://doi.org/10.1093/mnras/staa3764)
- Zhou, R., Dey, B., Newman, J. A., et al. 2023, *AJ*, 165, 58, doi: [10.3847/1538-3881/aca5fb](https://doi.org/10.3847/1538-3881/aca5fb)
- Zou, H., Gao, J., Zhou, X., & Kong, X. 2019, *ApJS*, 242, 8, doi: [10.3847/1538-4365/ab1847](https://doi.org/10.3847/1538-4365/ab1847)
- Zou, H., Gao, J., Xu, X., et al. 2021, *ApJS*, 253, 56, doi: [10.3847/1538-4365/abe5b0](https://doi.org/10.3847/1538-4365/abe5b0)
- Zou, H., Sui, J., Xue, S., et al. 2022, *Research in Astronomy and Astrophysics*, 22, 065001, doi: [10.1088/1674-4527/ac6416](https://doi.org/10.1088/1674-4527/ac6416)
- Zwicky, F., Herzog, E., & Wild, P. 1963, *Catalogue of galaxies and of clusters of galaxies*, Vol. 2